Available online at www.sciencedirect.com
SCIENCE DIRECT®
Polymer 45 (2004) 3943–3952
polymer
www.elsevier.com/locate/polymer

Monte Carlo simulations on the effects of nanoparticles on chain deformations and reinforcement in amorphous polyethylene networks

Mohammed A. Sharaf[a,b,*], James E. Mark[a]

[a]Department of Chemistry and the Polymer Research Center, The University of Cincinnati, Cincinnati, OH 45221-0172, USA
[b]Department of Chemistry, Helwan University, Ain Helwan, Cairo 11795, Egypt

Received 20 June 2003; received in revised form 17 February 2004; accepted 17 February 2004

Abstract

Reinforcing effects in an amorphous polyethylene matrix were estimated for spherical filler particles arranged either on a cubic lattice or randomly in space. Attention was first focused on the effects of the type of arrangement of the particles on the microscopic properties of the polymer chains. Specifically, Monte Carlo rotational isomeric state (MC-RIS) simulations were carried out to predict the effects of the volumes excluded by the filler particles on the configurational distribution functions of the chains, and from these distributions the elastomeric properties of the composites. The calculations were carried out for a range of particle sizes and particle volume fractions. As expected, filler inclusions are found to increase the non-Gaussian behavior of the chains. The results were compared with those from small-angle neutron scattering (SANS) experiments. In the case of arrangement on a cubic lattice, chains dimensions were always found to decrease. In the randomly-dispersed filler arrangements, there were significant increases in chain dimensions relative to the unfilled system in some instances, and the changes were in excellent agreement with the SANS results. The present simulations thus give further encouragement to interpretations of chain deformations in filled systems in terms of volume exclusion effects from the nanoparticle inclusions, including their dispersions and arrangements within polymer matrices.

Keywords: Monte Carlo methods; Rotational isomeric states (RIS); Reinforcement

1. Introduction

Many commercial polymeric materials are composites and are successfully used in many demanding applications [1–5]. In such composite materials, addition of rigid particles to polymers can produce a number of desirable effects, such as improvements in mechanical properties. Such improvements are determined by (i) the properties of the components, (ii) the shapes, natures of the dispersions, and degrees of aggregation of the reinforcing particles (iii) the morphologies of the system, and (iv) the nature of the interfaces and interphases. An important property of the interface, which can greatly affect mechanical behavior, is the strength of the bonding between the host and the dispersed phases. Thus, enhancement of the modulus of a filled polymer results from complex interplays among the properties of the individual constituent phases; the matrix chains, the rigid inclusions, and the interfacial regions [1–5].

There are various models for predicting the properties of particulate-filled polymeric materials and the unusual 'stiffening' effects observed. Critical reviews of these theories are given by Ahmed and Jones [6], Edwards [7], and Wang [8]. In the terminologies in these models, the reinforcement is determined by the interfacial energies [6,9] and geometrical factors (namely, size, shape and volume fraction of the filler) [6–10]. The proposed mechanisms for the interactions between particulate fillers and the polymer matrix include: steric interactions [9,11], formation of temporary junctions [12], concentration of dispersions [13,14], generation of filler 'networks' [15], and overlap resistance of filler aggregates [16–18]. In related work, Wu et al. [19] performed Monte Carlo calculations for two-dimensional freely-jointed polymers in equilibrium with a random lattice of obstacles. Also, based on a generic finite element analysis, Gusev et al. [20–23] numerically

* Corresponding author. Address: Department of Chemistry, Helwan University, Ain Helwan, Cairo 11795, Egypt. Tel.: +20-2-555-2468; fax: +20-2-555-2468.
E-mail address: sharafma@yahoo.com (M.A. Sharaf).

0032-3861/$ - see front matter © 2004 Published by Elsevier Ltd.
doi:10.1016/j.polymer.2004.02.073

identified morphologies that provided ultra high shear moduli in multiphase materials comprising anisotropic, arbitrarily shaped, and oriented phases.

Recent studies using small-angle neutron scattering (SANS) are providing relevant information on filler-induced deformations of polymer chains [17,24–26]. Of particular relevance here is the neutron scattering studies by Nakatani et al. on silica-filled PDMS [25,26]. When the chain dimensions were approximately the same size as the filler particles, their scattering results showed a decrease in chain dimensions at all filler concentrations. Chains with larger dimensions, however, showed increases in these dimensions, at least at low filler concentrations. These experimental results are in good semi-quantitative agreement with earlier Monte Carlo simulations in which spherical filler particles were placed either regularly (on a three-dimensional cubic lattice), or irregularly (in random arrangements throughout the volume in which the chains were subsequently generated) [27,28].

Over the past few years, polymeric systems filled with rigid nanoparticle inclusions have been the subject of a number of computer simulation studies [20–23,27–42]. Those by the present authors and their colleagues have focused on the nanoparticles deforming the matrix chains through their excluded volume effects [27–35]. The inabilities of the chains to penetrate the particles cause their dimensions to be either extended or compressed (relative to their initial dimensions in the absence of the particles). These deformations obviously affect the end-to-end chain distance distributions that are central to the calculation of elastomeric properties [24–48].

Vacatello [36–40] carried out some relevant simulations for dense polymer systems that gave results in disagreement with the increases of chain dimensions predicted from the earlier simulations and observed experimentally in the neutron scattering studies. It was concluded that that increased chain dimensions observed in neutron scattering experiments could not be explained on the basis of excluded volume arguments, and that simulations of filled polymer systems had to be performed in melt systems having realistic densities [36–40].

The fact that the two types of simulations gave different results prompted the present investigation, which extends some of the earlier simulations based on excluded volume effects. It focuses first on the distribution $P(r)$ of the end-to-end vector of a polymer chain, which is one of its most important characteristics [27–35,41–48]. This function tends to have a Gaussian form for long flexible chains, but the rigorous calculation of $P(r)$ is complicated for shorter chains, and even more so for polymer chains in the environment of filler particles. As has been already mentioned, if filler particles can cause the chains to be either extended or contracted, this will of course also change the force required for elastic deformations and thus elastic moduli [27–35,42–45]. Excluded-volume simulations of this type postpone treatment of other effects contributing to filler reinforcement such as matrix–filler and filler–filler interactions [27–35,42–45]. Thus, the present study addresses only the influence of volume excluded by the rigid nanoparticle inclusions as well as their mutual dispersion in the matrix on the microscopic properties of the matrix chain deformations. The distributions obtained from the simulations will be used in the standard rubberlike elasticity theory to estimate values of the modulus [27–35, 42–45]. At least qualitative comparisons will be made between these simulated values of the modulus and the most relevant experimental results.

2. The present theoretical model

The Monte Carlo rotational isomeric-state simulations were performed for amorphous polyethylene (PE) chains with degree of polymerization $n = 300$ at a temperature $T = 450$ K. The three-state rotational isomeric state RIS model was based on the usual form of the statistical weight matrix [49–51]:

$$U = [u_{\zeta\eta}] = \begin{bmatrix} 1 & \sigma & \sigma \\ 1 & \sigma\psi & \sigma\omega \\ 1 & \sigma\omega & \sigma\psi \end{bmatrix} \tag{1}$$

with $u_{\zeta\eta} = \exp(-E_{\zeta\eta}/RT)$ being the Boltzmann factor in the energy $E_{\zeta\eta}$ for a pair of skeletal bonds with bond $i-1$ being in the state ζ and ith bond in state η. *R is the gas constant*. These discrete states occur at torsion angles $\phi = 0°$, $120°$, $-120°$ corresponding to: *trans, gauche*$^+$*, and gauche*$^-$, respectively. The statistical weight parameters used in the calculations corresponded to $E_\sigma = 850$ cal/mol and $E_\omega = 1100$ cal/mol with, in addition, $\psi = 1$, and $\omega = 0$ [49–51].

Details of the generation of Monte Carlo chains and the modified Metropolis algorithm employed here are discussed in greater detail elsewhere [27–35]. The *apriori* probability matrix **P** and the conditional probability matrix **Q** have been the subject of an elaborate numerical treatments and detailed discussions [30–32].

Chains impinging on filler particles were discarded and the simulations continued until $N \geq 50,000$ acceptable Monte Carlo chains were accumulated. The resulting values of the end-to-end vector r were placed into a histogram to produce the desired end-to-end vector probability distribution function $P(r/r_{\max})$, with $r_{\max} = n\ell_0$, where ℓ_0 is the equilibrium bond length. This distribution function was obtained by accumulating the numbers of Monte Carlo chains having end-to-end distances within specified ranges. The function $P(r/r_{\max})$ was smoothed using cubic spline fits [27–34]. The smoothing procedure was necessary for the proper calculation of the stress-strain isotherms from the Monte Carlo histogram [27–34,43–45].

These results can be used directly in the Mark–Curro theoretical method [43–45] to calculate the elastic proper-

ties of the chains from the distribution functions $P(r/r_{max})$ of their end-to-end vectors. The distribution $P(r/r_{max})$ is directly related to the Helmholtz free energy $A(r)$ of a chain having the end-to-end distance r by [43–45,51]

$$A(r) = c - kT \ln P(r) \tag{2}$$

where k is Boltzmann constant and c is a constant. In this approximation, the three-chain model leads to the following general expression for the elastic free energy change during deformation [43–45,51]:

$$\Delta A = (\nu/3)[A(r_o\alpha_x) + A(r_o\alpha_y) + A(r_o\alpha_z) - 3A(r_o)] \tag{3}$$

Here, ν is the number of moles of chains in the network and $r_o = \langle r^2\rangle_o^{1/2}$ is the value of the root-mean-square (rms) end-to-end vector of the chains. The deformation ratio α_t relative to the dimension L_{it} at the start of the experiment is given for the case of isotropic deformation by [51]

$$\alpha_t = L_t/L_{it} \tag{4}$$

L_{it} should be clearly distinguished from L_{ot} (i.e. the length of the sample in the unfilled reference state).

In the case of filled networks, however, the deformation α relevant to the elastomeric matrix chains should be replaced by an effective mean amplified extension ratio α_{eff} due to the hydrodynamic effects of the inclusions, i.e. the disturbance of the strain distribution [52–54]:

$$\alpha_{eff} = (\alpha - 1)X_{eff} + 1 \tag{5}$$

For spherical inclusions, X_{eff} is a function of the volume fraction v_f of the inclusions and is given by [52–54]:

$$X_{eff} = 1 + 2.5v_f + 14.1v_f^2 \tag{6}$$

Thermodynamics provides the equation for the nominal stress f^* (defined as the elastic force at equilibrium per unit cross-sectional area of the sample in the undeformed state) [43–45,51]:

$$f^* = -T(\partial\Delta A/\partial\alpha)_T \tag{7}$$

Consequently, f^* is derived as a function $\ln P(r/r_{max})$, and $P' = \mathrm{d}[\ln P(r)]/\mathrm{d}r$. The smoothed function $P'(r/r_{max})$, together with the P'/P were obtained by cubic spline fits [27–34,43–45]:.

$$f^* = -(\nu kTr_0/3)[G'(r_0\alpha_{eff}) - \alpha^{-3/2}G'(r_0\alpha_{eff}^{-1/2})] \tag{8}$$

where $G(r) = \ln P(r)$, and $G('®r)$ denotes the derivative $\mathrm{d}G/\mathrm{d}r$. The IMSL subroutine 'CSDER' was used in the numerical calculations of the derivative of the smoothed function $P'(r/r_{max})$, together with the relationship $G' = P'/P$. The primary quantity of interest is the modulus or 'reduced stress' defined by [51]

$$[f^*] = \frac{f^*}{\alpha - \alpha^{-2}} \tag{9}$$

Since the modulus generally exhibits an unanticipated dependence on α, it is frequently represented in terms of the Mooney–Rivlin empirical equation

$$[f^*] = 2C_1 + 2C_2\alpha^{-1} \tag{10}$$

in terms of the constants $2C_1$ and $2C_2$ that are independent of the deformation ratio α [51].

The numerical calculations were performed for PE chains placed into a cubic lattice of spherical filler particles, as is schematically depicted in Fig. 1. For purposes of illustration, the calculated radius r_{efv} of a sphere representing the effective free volume available for the chains in the lattice as a function of the volume fraction of filler v_f is represented in Fig. 2 for different radii r_{sph} of the spherical nanoparticles. Fig. 3(a) and (b) depicts the polymer chain of interest now placed into a random arrangement of spherical filler particles. In order to test one of the possible criticisms of the earlier excluded-volume simulations [28], the randomness and non-bias of the present simulations was assured by frequently changing the nature of the particle dispersion in the lattice (generally after the successful generation of 200 chains).

The numerical calculations were performed for particles of different radii, specifically $r_{sph} = 1$ to 50 nm, and for a range of filler volume fractions ('loadings') $v_f = 0.0025$ to 0.6. In order to estimate the elastic properties, Monte Carlo RIS (MC-RIS) calculations were first applied for the free chains and then in the filled. Simulations were performed mainly at 450 K. It should be mentioned that the glass transition temperature T_g and the melting temperature T_m for low-density PE are approximately 253 and 388 K, respectively, [55].

A very large number of acceptable Monte Carlo chains ($N = 30,000–50,000$) were generated to acquire a

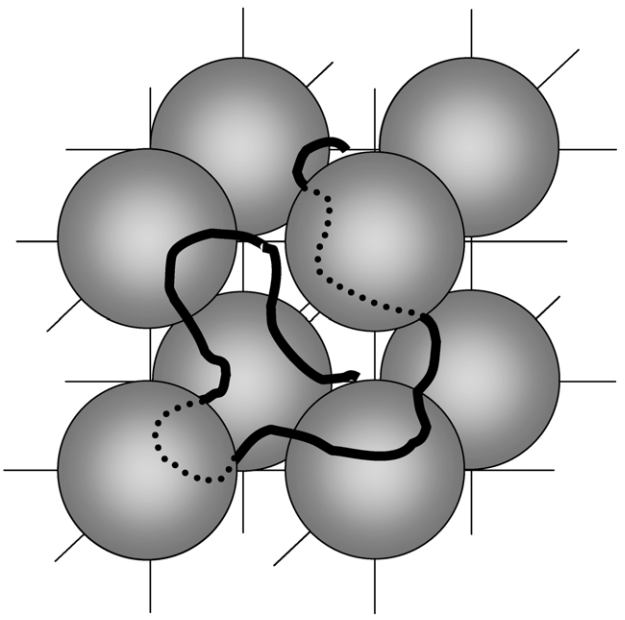

Fig. 1. Schematic view of a three-dimensional cubic lattice of spherical filler nanoparticles. Also shown is a polymer chain that has its origin and orientation in the lattice randomly generated among the particles.

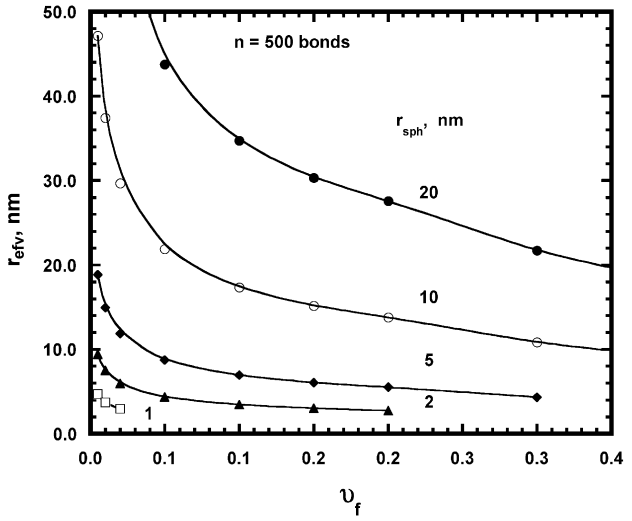

Fig. 2. The radius of a sphere representing the average effective free volume accessible by the chains within a unit cell shown as a function of the volume fraction of filler υ_f for spherical nanoparticles having the specified values of the radius r_{sph}.

sufficiently large statistical ensemble. In order to test another of the possible criticisms of the earlier simulations, the non-biased nature of the sampling was improved by randomly generated the chain origins in the lattice. Also, Euler's matrices were employed in order to have random orientations of chain axes during their generation. As was done before, any chain configuration having segments that overlapped with any of the lattice filler particles was rejected. In the earlier simulations, the methylene groups CH_2 had been treated as united atoms having a radius of 0.2 nm [33,34]. In the present improved simulations, however, the van der Waal's radii of all atoms were taken into consideration when checking for overlap between the filler particles and the polymer chain being generated.

3. Results and discussion

3.1. Particles arranged on a cubic lattice

Figs. 4 and 5 show the distributions of the end-to-end vector $P(r)$ as a function of r/r_{max} for PE chains having 500 bonds generated within a cubic lattice arrangement of rigid inclusions, having a range in volume fractions $\upsilon_f = 0.0025-0.6$. In Fig. 4, the spherical filler nanoparticles had a radius of 10 nm. For the purpose of clarity, only representative results are depicted. Each curve is labeled with the appropriate volume fractions υ_f, and the results for chains in the unfilled state are represented by the solid line. As has been generally the case, the chains in the lattice of spherical nanoparticles clearly manifest a shift to lower values of r/r_{max}. Also, it is important to note that the maximum becomes better defined than it is for the free chain. Apparently, this serves as a clear indication that the chains are compressed relative to the free chains in the unfilled state. At lower values of volume fractions (cf. $\upsilon_f = 0.025-0.02$), the distributions almost overlap entirely with that for the free chain. This could easily be described in terms of a preferential increase of the effective free volume available for the chains, as shown in Fig. 2. Thus, the chain dimensions would have been expected to increase.

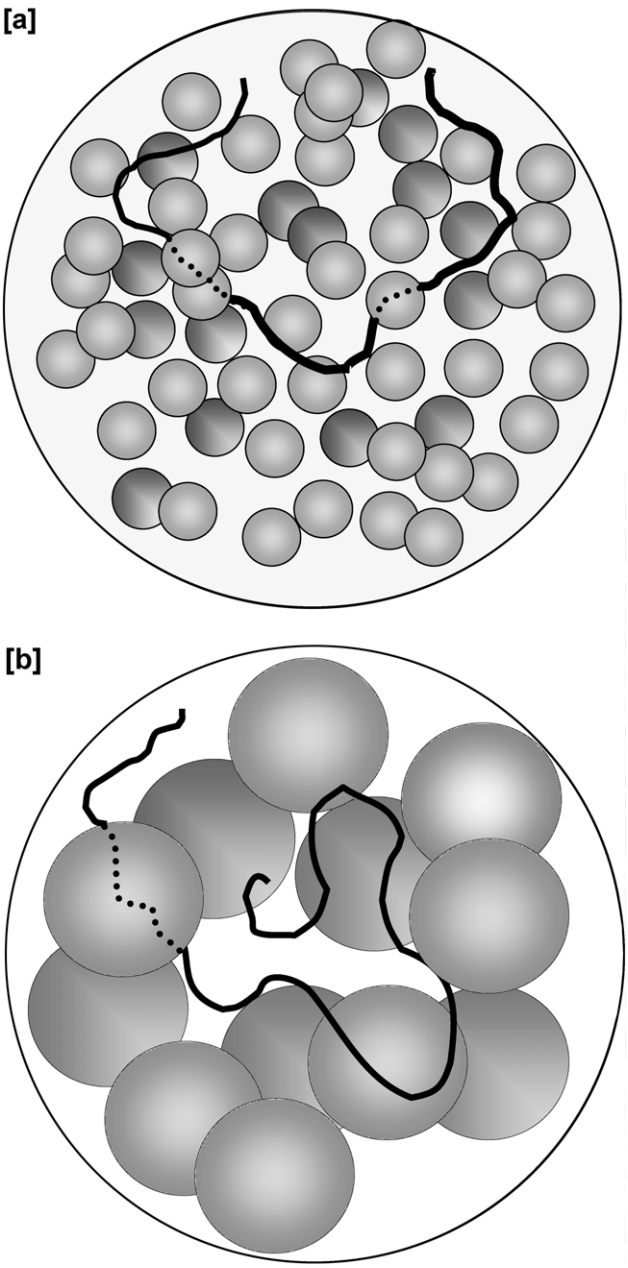

Fig. 3. Schematic view of a three-dimensional lattice of randomly dispersed small (a) and large (b) nanoparticles. Also shown is a polymer chain that has its origin and orientation in the lattice randomly generated among the spherical filler particles. Fig. 3(b) demonstrates how larger nanoparticles do result in higher values of the effective free volume fraction accessible to the chains than that provided by the smaller ones (Fig. 3(a)) at the same volume fraction.

Fig. 5 presents a clear demonstration of the effect of the filler particle size on these changes. The magnitude of the observed shift as r_{sph} increases is far less than that observed

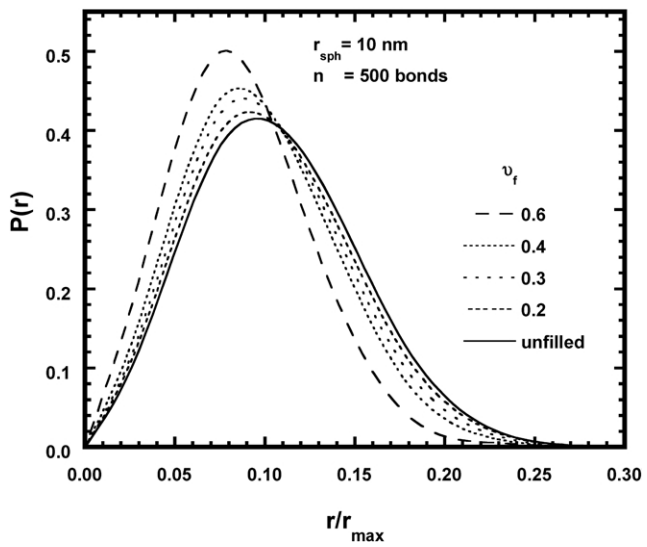

Fig. 4. Radial distributions $P(r)$ of the end-to-end vector r obtained by Monte Carlo simulations in a cubic lattice, shown as a function of the relative chain extension r/r_{max}. In this figure and the following ones, the results pertain to amorphous PE chains having 500 skeletal bonds, at 450 K, in the presence of fillers having the specified values of the volume fraction υ_f. Similarly, r_{sph} denotes the radius of the nanoparticles. The particular results shown here correspond to $r_{sph} = 10$ nm, and the solid line represents the results for the unfilled matrix polymer chain.

for the smaller filler particles (4 nm). Such differences are expected as a result of an increase of the lattice unit cell dimensions and corresponding increases in the free volume accessible to the chains with an increase in particle size, when the volume fraction of the filler is kept constant. This is also shown in Fig. 2. This clearly demonstrates the effects of particle size on the matrix polymer chains.

Of course, all the curves in Figs. 4 and 5 corresponding to higher loadings display significant deviations from that for the free chains and from Gaussian behavior in general. In other words, when the cubic unit cell dimension are greater than the root-mean-square end-to-end distance $\langle r^2\rangle_0^{1/2}$ of the polymer chains, the effects of the volume exclusion by the filler particles become negligible. As is readily apparent, there is a decrease in the effective free volume preferentially accessible to the chains with increase in the volume fraction of inclusions υ_f or a decrease in the inclusion size. Recent neutron scattering results are in excellent agreement with these simulated dimensional changes [27,31–35]. Unique distributions would be expected if the simulations were extended to lattices with $r_{sph} < 2$ nm. Unfortunately, most of the generated chain conformations overlap with filler particles and have to be rejected in this case, making the computer time needed for such simulations unacceptably long.

Fig. 6 presents values of the rms end-to-end distance as a function of the volume fraction of inclusions υ_f, (with $\upsilon_f = 0$ corresponding to the unfilled material). The results show that $\langle r^2\rangle_0^{1/2}$ for chains in lattices with spherical particles are significantly reduced in comparison to those in unfilled lattices. Again, and as would be expected, values of $\langle r^2\rangle_0^{1/2}$ for filler particles having initial $r_{sph} = 20$ nm are significantly higher than those for spherical particles with initial $r_{sph} = 2$ nm. These differences are expected as a result of an increase in the unit cell dimensions for a fixed value of υ_f. Most important, the results clearly demonstrate the effects of particle size on the distributions of the end-to-end vectors; at the same υ_f. Spheres having larger sizes lead to an increase in the effective free volume accessible within a unit cell.

The rms radii of gyration $\langle s^2\rangle_0^{1/2}$ and the characteristic ratio $C_\infty = \langle r^2\rangle_0/n\ell_0^2$ are given in Table 1. Values of the radii of gyration $\langle s^2\rangle_0^{1/2}$ and characteristic ratios C_∞ are found to follow the same trends seen in Fig. 6. Table 2 gives the corresponding results for random placements of the particles.

Fig. 7 shows the stress $f^*/\nu RT$ further normalized by the

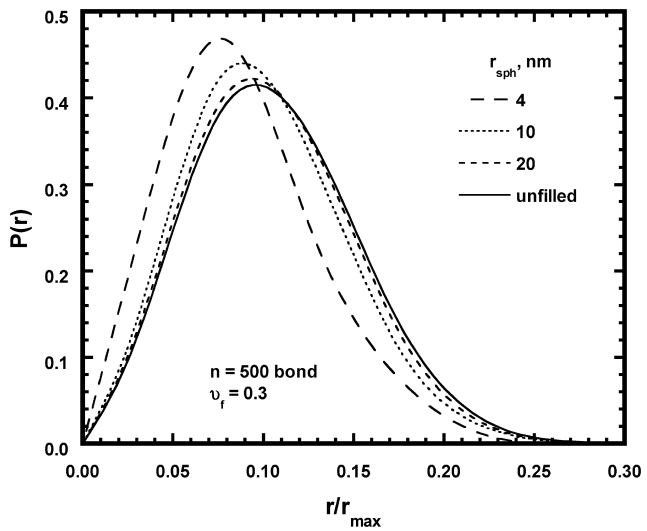

Fig. 5. Radial distributions for the case $\upsilon_f = 0.3$ and the specified values of r_{sph}, in a cubic lattice.

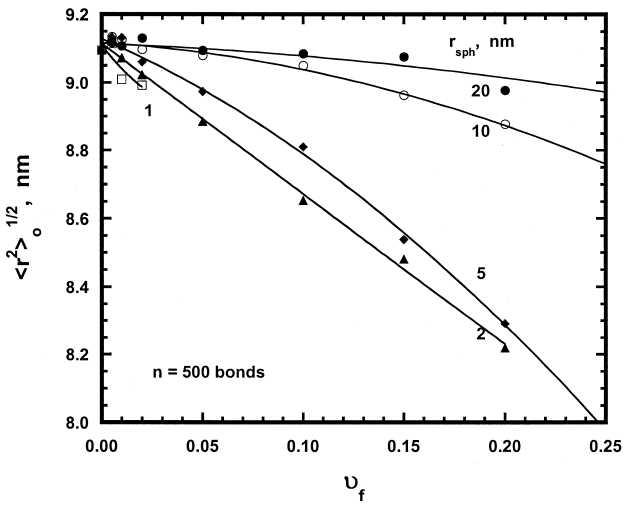

Fig. 6. Root-mean-square (rms) end-to-end distances $\langle r^2\rangle_0^{1/2}$ of the chains described in Fig. 4 as a function of the volume fraction of the nanoparticles having $r_{sph} = 10$ nm.

Table 1
Numerical results (450 K) for polyethylene chains having 500 skeletal bonds in a cubic lattice of spherical filler particles with diameters $r_{sph}>$

v_f [a]	r_{efv} [b] (nm)	$\langle r_0^2\rangle^{1/2}$ [c] (nm)	$\langle s_0^2\rangle^{1/2}$ [d] (nm)	C_∞ [e]
$r_{sph} = 20$ nm				
0.00	0.00	9.09	3.69	6.63
0.005	94.26	9.17	3.69	6.66
0.01	74.82	9.11	3.69	6.65
0.02	59.38	9.13	3.70	6.68
0.05	43.75	9.10	3.69	6.63
0.10	34.73	9.09	3.68	6.61
0.15	30.34	9.08	3.68	6.60
0.20	27.56	8.98	3.65	6.46
0.30	21.70	8.93	3.63	6.39
0.40	17.89	8.81	3.59	6.21
$r_{sph} = 10$ nm				
0.00	0.00	9.09	3.69	6.63
0.005	47.13	9.14	3.69	6.69
0.01	37.41	9.13	3.70	6.67
0.02	29.69	9.10	3.68	6.63
0.05	21.88	9.08	3.68	6.61
0.10	17.36	9.05	3.67	6.56
0.15	15.17	8.96	3.64	6.44
0.20	13.78	8.88	3.613	6.31
0.30	10.85	8.61	3.54	5.95
0.40	8.95	8.29	3.45	5.51
0.6	6.55	7.42	3.18	4.41
$r_{sph} = 4$ nm				
0.00	0.00	9.09	3.69	6.63
0.005	18.85	9.13	3.69	6.68
0.01	14.96	9.13	3.69	6.68
0.02	11.88	9.06	3.67	6.58
0.05	8.75	8.97	3.64	6.45
0.10	6.95	8.81	3.59	6.22
0.15	6.07	8.54	3.50	5.84
0.20	5.51	8.29	3.41	5.51
0.30	4.34	7.62	3.18	4.66
$r_{sph} = 2$ nm				
0.00	0.00	9.09	3.69	6.63
0.005	9.43	9.12	3.69	6.66
0.01	7.48	9.07	3.68	6.59
0.02	5.94	9.02	3.65	6.52
0.05	4.38	8.89	3.61	6.33
0.10	3.47	8.65	3.52	6.00
0.15	3.03	8.48	3.45	5.76
0.20	2.76	8.22	3.36	5.41
$r_{sph} = 1$ nm				
0.00	0.00	9.09	3.69	6.63
0.005	4.71	9.11	3.69	6.65
0.01	3.74	9.01	3.66	6.50
0.02	2.97	8.99	3.65	6.48
0.05	2.19	8.89	3.60	6.34

[a] Volume fraction of filler.
[b] Radius of an effective free volume sphere accessible to the polymer chain.
[c] Root-mean-square end-to-end distance (nm).
[d] Root-mean-square radius of gyration (nm).
[e] Characteristic ratio, $\langle r^2\rangle_0/n\ell^2$.

Table 2
Results for the same system as in Table 1, but with the filler particles randomly dispersed

v_f [a]	r_{efv} [b] (nm)	$\langle r_0^2\rangle^{1/2}$ [c] (nm)	$\langle s_0^2\rangle^{1/2}$ [d] (nm)	C_∞ [e]
$r_{sph} = 20$ nm				
0.0000	0.00	9.09	3.69	6.63
0.0025	118.76	9.04	3.66	6.55
0.005	94.26	9.01	3.65	6.50
0.01	74.82	9.03	3.66	6.53
0.02	59.38	9.01	3.65	6.50
0.05	43.75	9.02	3.65	6.52
0.10	34.73	9.00	3.64	6.49
0.15	30.34	8.92	3.63	6.38
0.2	27.56	8.93	3.62	6.39
0.3	21.70	8.86	3.60	6.29
0.4	17.89	8.80	3.57	6.21
0.5	15.18	8.58	3.51	5.90
$r_{sph} = 10$ nm				
0.0000	0.00	9.09	3.69	6.63
0.0025	59.38	9.18	3.69	6.75
0.005	47.13	9.14	3.68	6.68
0.01	37.41	9.12	3.67	6.66
0.02	29.69	9.18	3.67	6.75
0.05	21.88	9.11	3.65	6.66
0.10	17.36	8.99	3.62	6.48
0.15	15.17	8.81	3.57	6.21
0.2	13.78	8.75	3.55	6.13
0.3	12.16	8.71	3.54	6.07
0.4	8.95	8.16	3.35	5.34
0.5	7.59	7.99	3.29	5.12
$r_{sph} = 4$ nm				
0.0000	0.0000	9.09	3.69	6.63
0.0025	23.75	9.23	3.70	6.82
0.005	18.85	9.24	3.70	6.85
0.01	14.96	9.28	3.70	6.91
0.02	11.88	9.36	3.69	7.02
0.05	8.75	9.37	3.66	7.04
0.10	6.95	9.01	3.54	6.51
0.15	6.08	8.69	3.45	6.05
0.2	5.51	8.47	3.38	5.75
$r_{sph} = 2$ nm				
0.00	0.0000	9.09	3.69	6.63
0.0025	11.876	9.57	3.76	7.34
0.005	9.4262	9.83	3.79	7.74
0.01	7.4816	10.29	3.86	8.48
0.02	5.9381	10.55	3.89	8.92
0.05	4.3753	10.83	3.91	9.39
0.075	3.8221	10.25	3.77	8.42
0.1	3.4726	9.96	3.69	7.95
$r_{sph} = 1$ nm				
0.00	0.00	9.0940	3.69	6.63
0.0025	5.94	10.194	3.85	8.33
0.005	4.71	11.154	4.02	9.97
0.01	3.74	11.087	3.99	9.85
0.02	2.97	11.744	4.10	11.05

[a] Volume fraction of filler.
[b] Average radius of an effective free volume sphere accessible to the polymer chain.
[c] Root-mean-square end-to-end distance (nm).
[d] Root-mean-square radius of gyration (nm).
[e] Characteristic ratio, $\langle r^2\rangle_0/n\ell^2$.

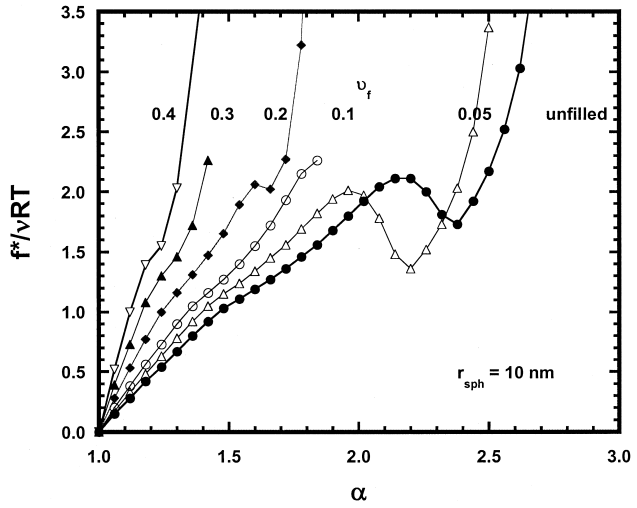

Fig. 7. Normalized stress shown as a function of the elongation α, at the start of the experiment, for the case $r_{sph} = 10$ nm and for the specified values of υ_f, in a cubic lattice.

number ν of chains as a function of the apparent macroscopic elongation α. It was calculated from Eq. (8), as is customarily done. In Fig. 8, the reduced modulus $[f^*]/\nu RT$ is illustrated as a function of reciprocal elongation α^{-1}, calculated according to Eq. (9). The representation is that suggested by the Mooney–Rivlin relationship [51], and the results are for the chains described in Fig. 4. The unusual maxima and minima are pathological and are a clear indication that a slight change in the shape of the distribution function near r_0 has a pronounced effect on the stress–strain behavior. The effect might also be related to the histogram method employed here. The proper calculation of the distribution function near r_0 might require histograms with smaller intervals around r_0 [27,31–35, 43–45].

In any case, at small strains an increase in the normalized longitudinal modulus is observed for chains filled with

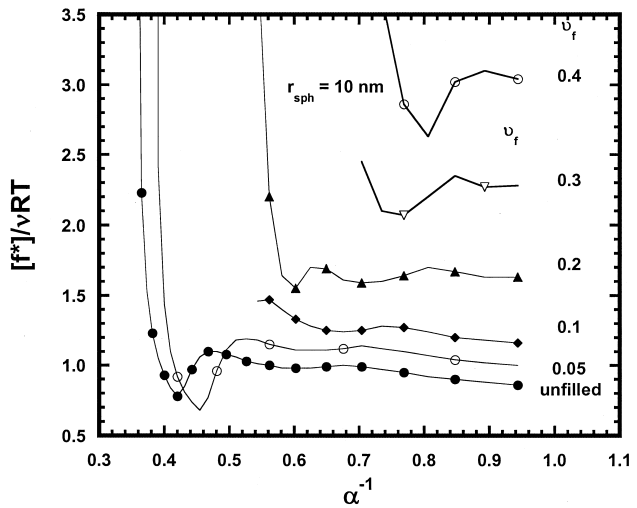

Fig. 8. The comparisons made in Fig. 7, but now for the normalized moduli shown as a function of the inverse elongation α^{-1}.

spherical nanoparticles (above that for the free chains). This is shown in Fig. 8. The enhancement in the small-strain modulus is estimated to be higher than 300%, and increases proportionally with an increase in particle loading. All of the isotherms in these figures show upturns in modulus as elongation increases, and such non-Gaussian behavior is clearly a result of the finite extensibility of the chains. More specifically, these upturns are due to the rapidly diminishing number of configurations at larger values of r. This is, correspondingly, accompanied by significant decreases in the entropy of the chains, with a corresponding increases in $[f^*]$. Such increases are more pronounced for composites having higher υ_f. In agreement with a wealth of experimental data, increases in modulus $[f^*]$ above those for the free chains is clearly apparent, in particular at small strains. An increase in loading, υ_f, results in a decrease in the unit cell dimensions, at fixed r_{sph}. As is demonstrated in Figs. 7 and 8, and as was expected from Fig. 4, chains in lattices having higher particle loadings also show a decrease in the elongation at which the upturn in the modulus occurs. This is an expected result of the diminished values of $\langle r_0 \rangle$. Again with decreasing volume fraction υ_f (i.e. with increasing unit cell dimension at fixed r_{sph}), the nominal stress approaches the limit of a free chain. In this connection, it is noteworthy that the stress-strain behavior depends on both the volume fraction and particle size, and subsequently on the specific shape of the end-to-end distribution function near $\langle r_0 \rangle$, according to Eq. (8) [27–35,43–45]. Deviations from the Mooney–Rivlin predictions can easily be attributed to slight changes in the shape of the distribution function near $\langle r_0 \rangle$ [27–35,43–45]. Even at equivalent values of $\langle r_0 \rangle$, it has been found that the shapes of the stress–strain curves could be entirely different [27–35,43–45].

The main point here is that the moduli obtained are larger than those for unfilled networks, in particular at low extensions. Furthermore, it is clear that a slight change in the particle size, and correspondingly in the unit cell dimensions, has significant effects on the modulus. It should be noted that for Gaussian chains the modulus $[f^*]/\nu RT$ is independent of elongation, and has a value of unity. One should note that Gaussian-like behavior is expected to prevail at lower elongations.

In Fig. 9, the modulus is shown as a function of the effective elongation α_{eff}.rather than the apparent elongation α. As would be expected, when account is taken of the inherent amplification of strain (overstrain) due to hydrodynamic effects accompanying the presence of particles, the reduced moduli $[f^*]$ approach that of the free chain, regardless of the volume fraction of filler. Thus, the simulations unambiguously demonstrate effects of the non-uniform stress fields around the particles on the deformation of the matrix chains.

3.2. Particles dispersed randomly

In this case, the PE matrix chains were introduced into a

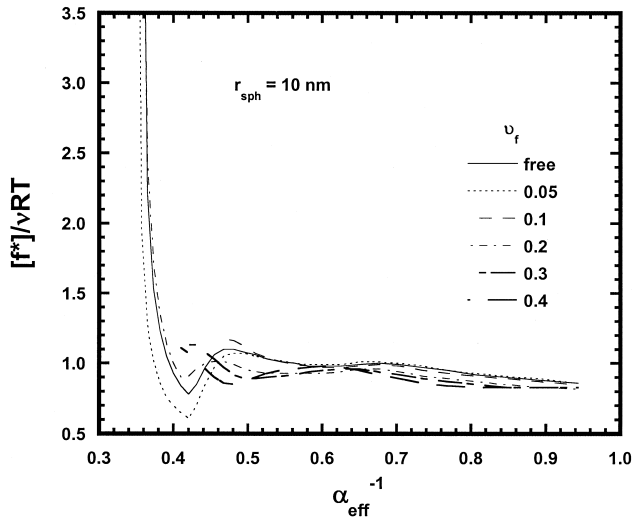

Fig. 9. The comparisons made in Fig. 8, but now shown a s a function of inverse effective elongation α_{eff}^{-1} that accounts for strain amplification induced by the nanoparticle inclusions.

random dispersion of non-overlapping spherical nanoparticles. Figs. 10 and 11 shows the distributions obtained from these numerical calculations, and Fig. 12 shows the chain dimensions. The characteristic and most distinctive features of Fig. 12 are the obvious increases in the root mean square end-to-end (relative to those of the unfilled ones). In some instances, the increase is substantial. It is clearly apparent that the magnitude of the increase is strongly affected by the volume fraction and/or the size of the nanoparticles. The results obtained for the end-to-end distances show a maximum before a decrease in values, with increase in filler concentration. This is reflected in the distribution functions resulting from these simulations as is shown in Fig. 11. With decrease in nanoparticle size, the distribution shifts to higher values of $r/r_{\max}$, i.e., towards more stiffened (extended) chain conformations with higher values of $\langle r_0 \rangle$.

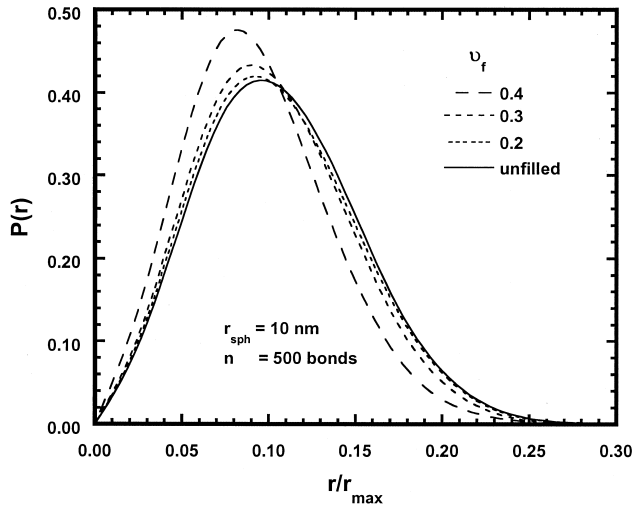

Fig. 10. Some of the comparisons made in Fig. 4, but now for chains generated in a lattice of randomly dispersed non-overlapping spherical nanoparticles.

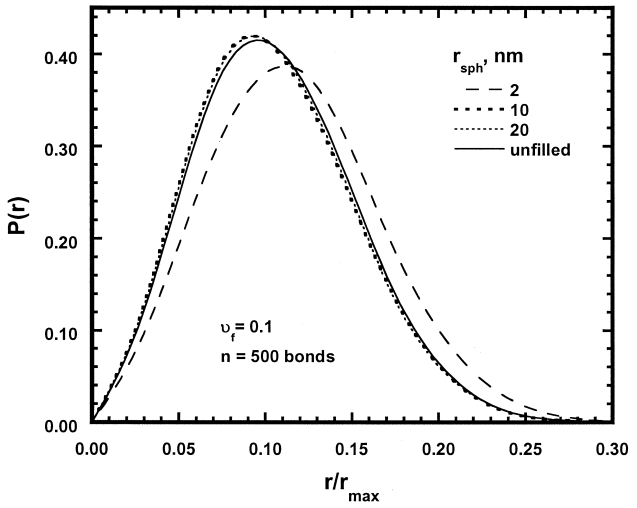

Fig. 11. Some of the comparisons made in Fig. 5, but now for $\upsilon_f = 0.1$, in a lattice of randomly dispersed non-overlapping spherical nanoparticles.

Such behavior is again expected in view of the inevitable effective free volume accessible to the chains, as has been already discussed.

In this context, it is important to note that the random dispersion of inclusions in contrast to the regular arrangement could lead to some aggregates with the development of some chains of filler particles, even in the undeformed state [15,53] Also, an increase in the concentration of inclusions could lead to a network interpenetrating the polymer ('filler networking') [15,53]. At higher loadings ($\upsilon_f > 0.3$), the inclusions become less diluted by the matrix chains, leading to percolation behavior that has been widely documented both experimentally and theoretically in the case of carbon black [15,53].

Such results are in excellent agreement with the most recent neutron scattering results. This is a clear indication of changes in the accessible effective free volume with changes in loading υ_f [27–35]. At sufficiently lower

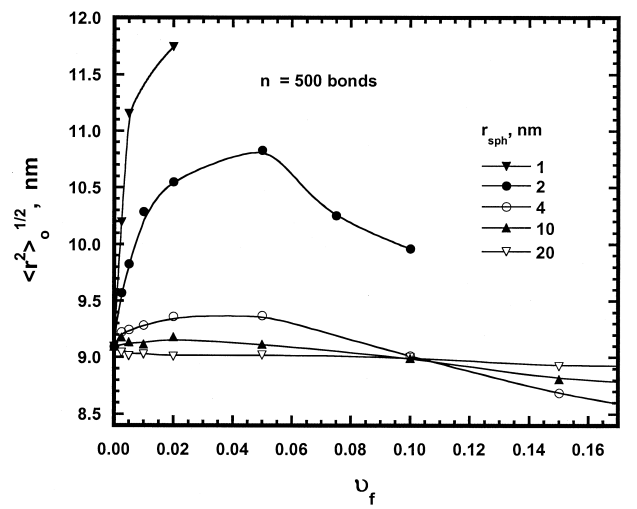

Fig. 12. The comparisons made in Fig. 6, but now for a lattice of randomly dispersed non-overlapping spherical nanoparticles.

loadings and smaller particle sizes, a considerable expansion in chain dimensions is observed. This could be owing to an inevitable substantial increase in the number of inclusions as their size is decreased; at a certain volume fraction v_f (cf. Fig. 3(a)) [25–27–35]. Consequently, the chain is forced to adopt more extended configurations that results in a type of 'strain amplification', before the application of mechanical deformation [24–35]. With an increase in volume fraction v_f of particles, it is apparent that the nanoscopic inclusions could certainly aggregate and interconnect. As a result, the effective free volume accessible to chain trajectories between the obstacles decreases drastically and more compact configurations have to be adopted by the chains. Undoubtedly, this results in compression of chain dimensions in order for a chain to fit within a certain accessible volume [25–27–35]. Such behavior is more pronounced with an increase in the particle size and v_f.

In Table 2, apparent and substantial increases are observed in the rms radius of gyration. Values of the characteristic ratio C_∞ of the chain dimensions relative to those of a freely-jointed chain follow the same trend. Again, this increase is strongly affected by the volume fraction of the filler and/or the size of the particles. The results obtained show discernible maxima before decreasing in value with increase in filler concentration. Simulations showing the general trend of reduction in chain dimensions will be presented elsewhere. They are consistent with our previous results [27,31–35] and with those recently reported by Vacatello [36–40].

4. Conclusions

In summary, it should be emphasized that only certain volume fractions and dimensions of the nanoparticles result in an increase in chain dimensions. This is quite important in efficient utilization of nanofillers in polymeric systems. In addition, our new results provide further support to those observed in neutron scattering experiments, specifically an increase followed by a decrease in chain dimensions. This provides further evidence regarding the efficiency and sensitivity of single-chain simulations in characterizing effects of filler environments on host elastomeric chains. These simulations are considered more accurate since the detailed internal structure of the chain units is not neglected, as is generally the case in dense simulations.

In addition, the numerical results presented are in qualitative agreement with experimental values of moduli reported in the literature for a wide range of filled systems [4,6]. Quantitative comparisons are difficult in view of the fact that the present simulations are concerned only with effects of volumes excluded by the filler particles.

In a more rigorous and comprehensive treatment of the this complex phenomenon of reinforcement, it is essential to focus on mechanisms of filler–matrix interactions that are dependent on the detailed structure of the surface as well as filler–filler interactions that come into play with increased deformation. A combination of micromechanics of composites, mesoscopic modeling, and perhaps atomistic modeling would provide a unified molecular understanding and approach of the very complex behavior of multiphase composites. There are now concerted efforts towards that very goal [27–42,56,57].

Acknowledgements

It is a pleasure to acknowledge the financial support provided by the National Science Foundation through Grants DMR-0075198 (Polymers Program, Division of Materials Research), and INT-9605191 and INT-0111334 (US-EGYPT International Programs). It was also a pleasure to prepare this manuscript for the special issue of Polymer honoring Dick Boyd, who has long been a leading figure in the area of computations on polymeric materials.

References

[1] Christensen RM. Mechanics of composite materials. New York: Wiley; 1991.
[2] Boonstra BB. Polymer 1979;20:691.
[3] Ahmed S, Jones FR. J Mater Sci 1990;(25):4933.
[4] Kraus G. Adv Polym Sci 1971;8:155.
[5] Saam JC. Mater Res Soc Symp Proc 1992;91:274.
[6] Ahmed S, Jones FR. J Mater Sci 1990;25:4933.
[7] Edwards CJ. J Mater Sci 1990;25:4175.
[8] Wang M-J. Rubber Chem Technol 1998;71:520.
[9] Vidal A, Donnet JB. Prog Colloid Polym Sci 1987;75:201.
[10] Medalia AI. Rubber Chem Technol 1987;60:45.
[11] Maier P, Goeritz D. Kautsch Gummi Kunstst 1996;49:18.
[12] Cohen-Addad JP. Polymer 1992;33:13.
[13] Jones DAR, Leary B, Boger DV. J Colloid Interface Sci 1991;147:479.
[14] Payne AR, Whittaker RE. Rubber Chem Technol 1971;44:440.
[15] Witten TA, Rubinstein M, Colby RH. J Phys II 1993;3:367.
[16] Mullins L. Rubber Chem Technol 1969;42:339.
[17] Rharbi B, Cabane A, Vacher M, Joanicot M, Boue F. Europhys Lett 1999;46:472.
[18] Oberdisse J, Rhrabi Y, Boue F. Comp Theor Polym Sci 2000;10:207.
[19] Wu D, Hui K, Chandler D. J Chem Phys 1992;96:835.
[20] Gusev AA. Macromolecules 2001;34:3081.
[21] Lusti HR, Karmilov IA, Gusev AA. Soft Mater 2003;1:115.
[22] Gusev A, Rozman MG. Comput Theor Polym Sci 1999;9:335.
[23] Gusev AA, Karmilov IA. Macromol Theory Simul 2002;11:247.
[24] Westermann S, Kreitschmann M, Pyckhout-Hintzen W, Richter D, Straube E, Farago B, Goerigk G. Macromolecules 1999;32:5793.
[25] Nakatani AI, Chen W, Schmidt RG, Gordon GV, Han CC. Polymer 2001;42:3713.
[26] Nakatani AI, Chen W, Schmidt RG, Gordon GV, Han CC. Int J Thermophys 2002;23:199.
[27] Sharaf MA, Kloczkowski A, Mark JE. Comp Polym Sci 1994;4:29.
[28] Yuan W, Kloczkowski A, Mark JE, Sharaf MA. J Polym Sci, Part B: Polym Phys 1996;34:1647.
[29] Kloczkowski A, Sharaf MA, Mark JE. Comp Polym Sci 1993;3:39.
[30] Kloczkowski A, Sharaf MA, Mark JE. Chem Engng Sci 1994;9:2889.

[31] Sharaf MA, Kloczkowski A, Mark JE. Comp Theor Polym Sci 2001; 11:251.
[32] Sharaf MA, Mark JE. Polymer 2002;43:643.
[33] Sharaf MA, Kloczkowski A, Jacob KI, Mark JE. Polym Mater Sci Engng 2003;88:94.
[34] Sharaf MA, Mashali KB, Hammam M, Abdel-Ghani SA, Jacob KI. Polym Mater Sci Engng 2003;88:38.
[35] Sharaf MA, Abouhussein RH. Polym Prepr 2003;44:1258.
[36] Vacatello M. Macromolecules 2003;36:3411.
[37] Vacatello M. Macromolecules 2002;35:8191.
[38] Vacatello M. Macromolecules 2001;34:1946.
[39] Vacatello M. Macromol Theory Simul 2003;12:86.
[40] Vacatello M. Macromol Theory Simul 2002;11:53.
[41] Hanson DE. J Chem Phys 2000;113:7656.
[42] Zhang L, Xia A, Wang X, Ye G, Zhao D. Eur Polym J 2002;38:20633.
[43] Mark JE, Curro JG. J Chem Phys 1983;(79):5705.
[44] Curro JG, Mark JE. J Chem Phys 1984;80:4521.
[45] Curro JG, Schweizer KS, Adolf D, Mark JE. Macromolecules 1984; 80:4521.
[46] Zhang L, Xia A, Jiang Z, Zhao D. Macromol Theory Simul 2001;10: 651.
[47] Zhang L, Huang Y, Zhao D. Macromol Theory Simul 2001;10:479.
[48] Heinrich G, Vilgis TA. Macromolecules 1993;26:1109.
[49] Flory PJ. Statistical mechanics of chain molecules. New York: Interscience; 1969.
[50] Mattice WL, Suter UW. Conformational theory of large molecules. New York: Wiley-Interscience; 1994.
[51] Rehahn M, Mattice WL, Suter UW. Adv Polym Sci 1997;131/132:1.
[52] Erman B, Mark JE. Rubberlike elasticity. A molecular primer. New York: Wiley-Interscience; 1988.
[53] Guth E, Gold O. Phys Rev 1938;53:322.
[54] Guth E. J Appl Phys 1945;16:20.
[55] Smallwood HM. Appl Phys 1944;15:758.
[56] Mark JE. Polymer data handbook. New York: Oxford University Press; 1999.
[57] Ozmusul MS, Picu RS. Polym Compos 2002;23:110.